

Mathematical and simulation modeling of dual active bridge

Roman BARLIK, Piotr GRZEJSZCZAK, and Mikołaj KOSZEL*

Warsaw University of Technology, Warsaw, Poland

Abstract. The paper is a structured, in-depth analysis of dual active bridge modeling. In the research new, profound dual active bridge converter (DAB) circuit model is presented. Contrary to already described idealized models, all critical elements including numerous parasitic components were described. The novelty is the consideration of a threshold voltage of diodes and transistors in the converter equations. Furthermore, a lossy model of leakage inductance in an AC circuit is also included. Based on the circuit equations, a small-signal dual active bridge converter model is described. That led to developing control of the input and output transfer function of the dual active bridge converter model. The comparison of the idealized model, circuit simulation (PLECS), and an experimental model was conducted methodically and confirmed the high compatibility of the introduced mathematical model with the experimental one. Proposed transfer functions can be used when designing control of systems containing multiple converters accelerating the design process, and accurately reproducing the existing systems, which was also reported in the paper.

Key words: dual active bridge; small-signal analysis; averaged model; transfer function; parasitics; PI controller.

LIST OF SYMBOLS

E_1, E_2 – DC voltages (steady-state values),
 E_2' – circuit voltage E_2 reflected in the voltage of side,
 v_1, v_2 – alternating voltages of both bridges,
 $f_s = 1/T_s$ – frequency and period (T_s) of transistor switches equal to the frequency and period of alternating voltages v_1 and v_2 of both bridges,
 L_{eq}, R_{eq} – resultant inductance and resistance of the AC circuit, quantities reflected in circuit E_1 ,
 N_1, N_2 – the number of turns of the winding of the bridges H1, H2,
 $n = N_2:N_1$ – transformer turn ratio,
 d – the coefficient of phase shift between alternating voltages v_1 and v_2 of both bridges H1 and H2,
 $\varphi = d\pi$ – the angle of phase shift between the alternating voltages of both bridges H1 and H2,
 $T = T_s/2$ – the period of current changes in the DC circuits of both bridges,
 R_{1T}, R_{2T} – resistances of transformer windings,
 L_{1T}, L_{2T}, L_μ – winding leakage inductance, and transformer magnetizing inductance,
 R_s – resistance of the transistor in the conduction state,
 V_0 – threshold voltage of a diode or transistor,
 $R_{E1}, L_{E1}, R_{E2}, L_{E2}$ – filtering resistances and inductances of DC circuits E_1 and E_2 , respectively,
 $i_{d1}, i_{d2}, v_{d1}, v_{d2}$ – instantaneous values of currents and voltages in the DC circuits of both bridges H1 and H2, respectively,
 $i_{E1(AV)}, i_{E2(AV)}$ – average values for the period T (currents of circuits with source voltages E_1 and E_2 , changing as a function of time),

$i_{d1(AV)}, i_{d2(AV)}$ – average values for the period T of currents in DC circuits of bridge H1 and H2, respectively,

$v_{d1(AV)}, v_{d2(AV)}$ – the average values for the period T of voltages, in DC circuits of both bridges H1 and H2, changing as a function of time.

1. INTRODUCTION

A dual active bridge is one of the most used converters that couple two DC circuits, enabling bidirectional energy exchange and providing galvanic separation between these circuits. It is used primarily in systems with DC electricity storage [1,2] (batteries, supercapacitors), from which energy is consumed and then supplemented. The energy storage voltage may vary depending on its state of charge.

A dual active bridge consists of two single-phase H-type bridge inverters in which AC voltage circuits are connected via a medium- or high-frequency transformer and an inductor placed in the circuit with higher voltage (Fig. 1a).

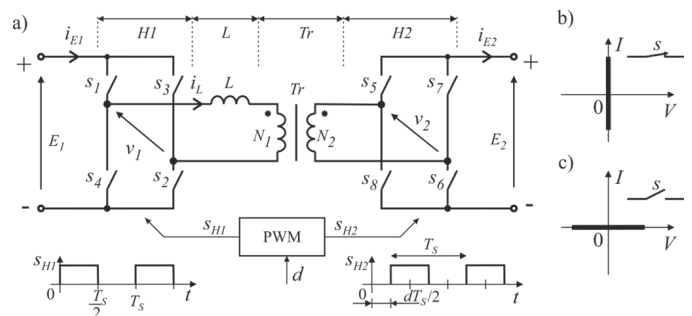


Fig. 1. Dual active bridge controlled by a phase shift of alternating voltages: a) simplified diagram of a circuit with a control unit; b), c) current-voltage characteristics of an ideal semiconductor switch in the on and off state, respectively

*e-mail: mikolaj.koszel@pw.edu.pl

Manuscript submitted 2022-03-18, revised 2022-06-25, initially accepted for publication 2022-07-25, published in October 2022.

Due to the transformer with the appropriate ratio $n = N_2:N_1$, correct operation of the system is ensured even with significantly different voltages of the coupled direct current circuits E_1 and E_2 . The alternating voltages of both bridges usually have the shape of positive and negative rectangular pulses lasting for the half-period of the $S_1 \div S_8$ switching time. The energy flow between the DC circuits is controlled by changing the phase shift between the alternating voltages of both bridges (H_1 and H_2). Energies flow towards the circuit whose rectangular voltage is lagging behind the voltage of another bridge. Disregarding the resistances existing in the real system, the instantaneous values of the transformer winding currents have linear changes with time, with constant derivatives equal to $\pm(E_1 + E_2)/L_{eq}$ or $\pm(E_1 - E_2)/L_{eq}$, respectively in the range $0 \leq t < dT$ and $dT \leq t < T$ (Fig. 2). Disregarding the power losses in the converter, the power transferred in the steady state between the coupled circuits can be described by formula (1) [3]

$$P = \frac{E_1 E_2}{2n f_s L_{eq}} d(1-d) = \frac{E_1 E_2'}{2 f_s L_{eq}} d(1-d). \quad (1)$$

At given voltages E_1 and E_2 , power P is determined by the average values of currents in the DC circuits of both bridges. What is interesting is the relationship between the control signal d and the currents I_{E1} and I_{E2} . In the case of an ideal converter, equations (2) and (3) give

$$I_{E1(AV)} = \frac{E_2}{2n f_s L_{eq}} d(1-d), \quad (2)$$

$$I_{E2(AV)} = \frac{E_1}{2n f_s L_{eq}} d(1-d), \quad (3)$$

where: E_1, E_2 – voltages of direct current circuits; E_2' – circuit voltage E_2 reflected in the voltage side E_1 ; $f_s = 1/T_s$ – switch-

ing frequency of transistors equal to the frequency of alternating voltages of both bridges; L_{eq} – resultant inductance of the alternating current circuit equal to the sum of the inductance of the choke and the leakage inductance of the transformer reflected in the circuit E_1 ; $n = N_2/N_1$ – transformer ratio; d – coefficient of phase shift between alternating voltages v_1 and v_2 .

It should be noted that the currents in the DC circuits of both bridges have a period equal to $T = T_s/2$.

The literature on the analysis of static and dynamic properties of DAB systems is extensive [4–7]. Undoubtedly, the most accurate results are obtained using computer programs designed to simulate power electronic circuits (PSPICE, SABER, PLECS), but the calculations are very time-consuming, especially in the case of transient processes. Hence, various simplified descriptions of converters are developed to speed up the calculations, using large- and small-signal averaged models [2, 8–11, 13, 14].

Most publications on modeling DAB systems assume that the elements and components of the analyzed system are ideal, ignoring their resistances and threshold voltages. Only a few publications present averaged DAB models, taking into account some parasitic resistances of semiconductors and magnetic elements [15, 16]. The work [16] presents a large- and small-signal averaged model of a DAB system, in which only parasitic resistance parameters are taken into account: the resistance of transformer windings, diode and MOSFET resistances in conduction, resistances of snubbers, ESR of capacitors in DC circuits and filter inductor resistance in these circuits. In the equations describing the models, the threshold voltages of the body diodes were omitted. The threshold voltages of transistors, such as IGBT, which are used in the case of higher powers and higher voltages, are not considered, either [17, 18].

This paper presents a description of a large-signal and small-signal averaged DAB model, in which the model given in [16] was supplemented with threshold voltages of diodes and transistors as well as a leakage inductor inductance and AC resistance. The inductor, in most cases, must be included in the AC circuit to obtain the correct control range of the power transferred between the E_1 and E_2 circuits. The description is supplemented with a full equivalent diagram of inductive components.

Section 2 describes the DAB system model, which includes the most significant parasitic parameters of the system components and components. The equations describing the instantaneous values of the currents in the alternating current circuits of both bridges are given, taking into account the resistance of the switches and the winding resistance of the magnetic elements. In Section 3, the averaged model of the DAB is presented, whereas the transfer functions in the domain of the complex variable “s” are given in Section 4. In Section 5, to check the influence of parasitic parameters, an analysis of the averaged model with ideal elements was performed [12, 19]. Simulation and experimental models, which were developed to verify the discussed model, are presented in Sections 6 and 7. They are followed by the presentation of the results, comparison (Section 8), and conclusion (Section 9).

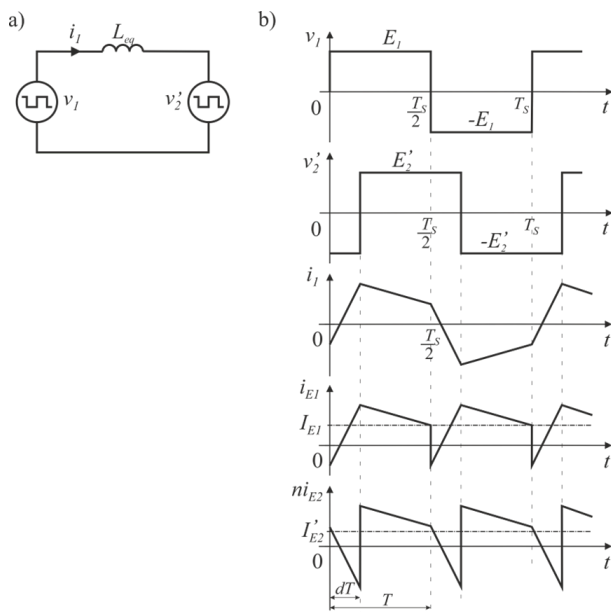


Fig. 2. DAB AC circuit: a) equivalent diagram; b) voltage and current waveforms ($v_2' = v_2/n$ – secondary side voltage of the transformer reflected in the primary side)

2. CIRCUIT MODEL OF A REAL DAB CONVERTER

In real DAB converters, besides the elements shown in Fig. 1, LC filters and RC in DC circuits are also used. Figures 3a and 3b show a diagram of the DAB system, which includes the basic parameters of realistic elements and components, including:

- Windings resistances R_{1T} and $R'_{2T} = R_{2T}/n_2$ of the transformer at the current frequency equal to f_s [20].
- The resistances of semiconductor switches R_s in the conduction state and their threshold voltages U_0 in the case of MOSFET transistors, only the resistance R_s should be taken into account, equal to the channel resistance R_{ON} (Figs. 3c and 3d), it was assumed that all switches have the same resistance R_s and the same threshold voltages, where $R'_s = R_s/n_2$ and $V'_0 = V_0/n$ (Figs. 3c and 3d).
- Leakage inductor winding resistance R_L for alternating current with frequency f_s .
- Resistances of resistors in RC snubber circuits (including series ESR of capacitors R_1 and $R'_2 = R_2/n_2$ in DC circuits).
- Inductances and resistances of connections and filter chokes in the DC circuits R_{E1} , L_{E1} , and R_{E2} , L_{E2} reflected in the E_1 voltage circuit.

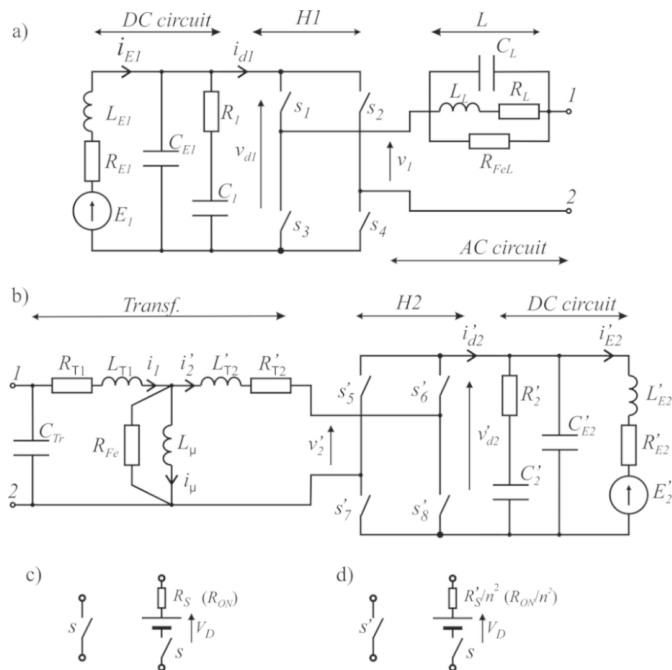


Fig. 3. Diagram of the DAB circuit including parasitic parameters (values and parameters related to the E_1 circuit side): a), b) circuit diagram; c), d) substitute diagrams of power electronic switches

This diagram ignores the influence of the parasitic capacitance C_p of the transformer ($i_{CTR} \ll i_1$), resistance R_{Fe} representing the power losses in the core of the transformer, choke ($i_{Fe} \ll i_1$), and the magnetizing inductance L_μ of the transformer ($i_\mu \ll i_1$) [21]. In contrast, the equivalent resistance and inductance R_{eq} and L_{eq} and rectangular alternating transformer windings voltages v_1 and v'_2 windings were considered. The

listed quantities describe the following dependencies:

$$L_{eq} = L_L + L_{1T} + L'_{2T} = L_L + L_{1T} + \frac{L_{2T}}{n^2}, \quad (4)$$

$$R_{eq} = 2R_s + R_L + R_{1T} + R'_{2T} + 2R'_s = 2R_s + R_L + R_{1T} + \frac{R_{2T} + 2R_s}{n^2}, \quad (5)$$

$$v_{10} = \pm (v_{d1} - 2V_0), \quad (6)$$

$$v'_{20} = \pm (v'_{d2} + 2V'_0) = \pm \frac{1}{n} (v_{d2} + 2V_0). \quad (7)$$

The equivalent diagram of the DAB system AC circuit with parameters reduced to the E_1 voltage circuit (assumed as the primary one) is shown in Fig. 4.

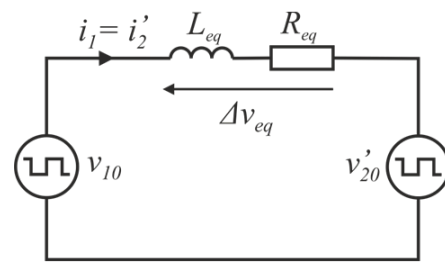


Fig. 4. Diagram of a DAB alternating current circuit with equivalent parameters R_{eq} , L_{eq}

It should be noted that the signs of the threshold voltages V_0 and V'_0 in formulas (6) and (7) depend on the direction of the energy flow (more precisely, the direction of the current flowing through the semiconductor switches). The signs adopted in the given formulas correspond to the control at which the energy is transferred from the source E_1 to the circuit E_2 . The formulas describing the power transferred between the DC circuits by the DAB converter, including the voltage drops on switches, can be found in [3], among others.

Assuming that the voltages v_{d1} and v_{d2} in the DC circuits of both bridges are constant (without ripple) and that $R_{eq} > 0$, the waveforms of the instantaneous values of the transformer currents (i_1 , i_2) in the steady state have the shape of exponential curves (Fig. 5). The waveforms of the instantaneous values of currents in the primary winding (i_1) and in the DC circuit (i_{d1}) are described by the following formulas and relations:

– in the range I ($0 \leq t < dT$)

$$i_1 = i_{d1} = A - a(A + I_I), \quad (8)$$

$$i'_{d2} = -i_{d1}. \quad (9)$$

– in the range II ($dT \leq t < T$)

$$i_1 = i_{d1} = B(1 - b) + I_{II}b, \quad (10)$$

$$i'_{d2} = i_{d1}, \quad (11)$$

where: $a = e^{-t/\tau}$; $b = e^{-(t-dT)/\tau}$; $\tau = L_{eq}/R_{eq}$; $A = (v_{10} + v'_{20})/R_{eq}$; $B = (v_{10} - v'_{20})/R_{eq}$ and I_I , I_{II} – instantaneous peak current values.

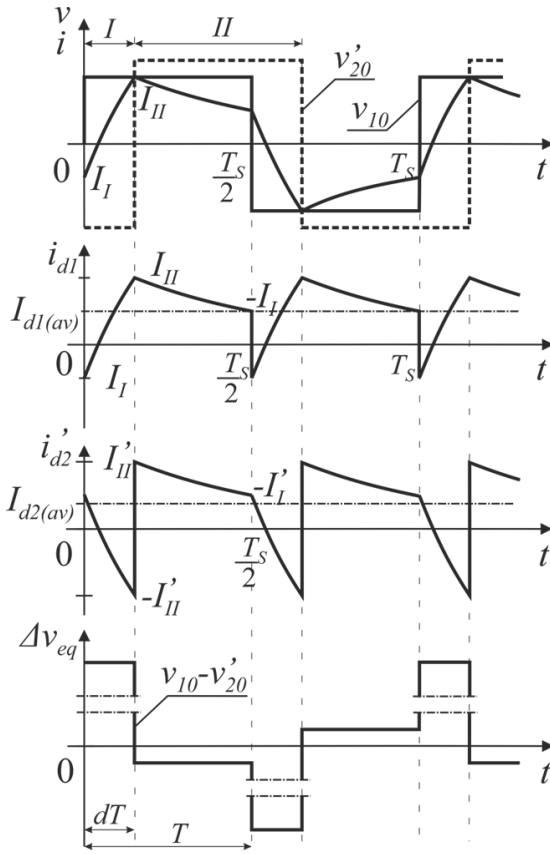


Fig. 5. The alternating voltage waveforms of both bridges v_{10} and v'_{20} (regarding the threshold voltages of semiconductor switches) and the current waveforms in the primary winding (i_1), and in the DC circuits of both bridges (i_{d1} , $i'_{d2} = ni_{d2}$) with emphasis on their exponential character (steady state)

The instantaneous extreme values of the I_I and I_{II} currents in AC and DC circuits are expressed by the formulas:

$$I_I = i_{d1}(T) = i_1(T) = \left(B + \frac{2}{R_z} v'_{20} e^{-\frac{T(1-d)}{\tau}} - A e^{-\frac{T}{\tau}} \right) \left(1 + e^{-\frac{T}{\tau}} \right)^{-1}, \quad (12)$$

$$I_{II} = i'_{d2}(dT) = i_1(dT) = \left(A - \frac{2}{R_z} v_{10} e^{-\frac{dT}{\tau}} + B e^{-T/\tau} \right) \left(1 + e^{-T/\tau} \right)^{-1}. \quad (13)$$

Based on formulas (8), (10), (12), and (13), it is possible to determine the average values of the currents in DC circuits ($i_{d1(AV)}$ and $i'_{d2(AV)}$) for the switching period of the instantaneous values.

$$i_{d1(AV)} = \frac{1}{T} \left[\int_0^{dT} i_{d1(I)} dt + \int_{dT}^T i_{d1(II)} dt \right] = Ad + B(1-d) + \frac{\tau}{T} (I_I + A) \left(e^{-dT/\tau} - 1 \right) + \frac{\tau}{T} (B - I_{II}) \left(e^{-T(1-d)\tau} - 1 \right), \quad (14)$$

$$i'_{d2(AV)} = \frac{1}{T} \left[\int_0^{dT} i'_{d2(I)} dt + \int_{dT}^T i'_{d2(II)} dt \right] = \frac{1}{T} \left[\int_0^{dT} (-i_{d1(I)}) dt + \int_{dT}^T i_{d1(II)} dt \right] = -Ad + B(1-d) - \frac{\tau}{T} (I_I + A) \left(e^{-\frac{dT}{\tau}} - 1 \right) + \frac{\tau}{T} (B - I_{II}) \left(e^{-T(1-d)\tau} - 1 \right) - \frac{u'_2}{R_{Fe}}. \quad (15)$$

In steady state, the mean values of currents and voltages in the DC circuits of both bridges in the successive half-periods $T = T_s/2$ do not change. After a disturbance, resulting e.g. from a change in the control factor (phase shift) d , the average values of the currents $i_{d1(AV)}$ and $i'_{d2(AV)}$ change from period to period. Assuming that the changes of the mean values take place much slower than the switching period ($T \gg T_s$), it can be assumed that the mean values, as slowly changing, change continuously and are a function of time (Fig. 6).

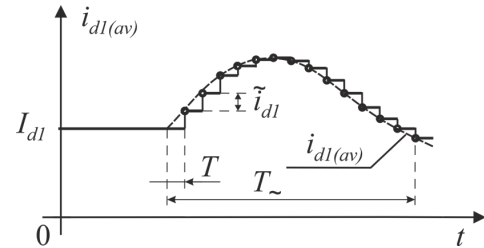


Fig. 6. Slow-changing oscillation ($T \gg T_s$) of the mean value of current $i_{d1(AV)}$ in the DC circuit of the bridge H_1 in the transient state; values changing discretely (stepped line) and mean values, as a continuous function of time, taken in the averaged DAB model (dashed line); \tilde{i}_{d1} – increment change of the average value of current $i_{d1(AV)}$ during the period $T = T_s/2$; I_{d1} – quiescent value in the DC circuit of the H_1 bridge

In the case of the DAB converter, the part of the circuit containing the H_1 bridge, L inductor, transformer Tr , and H_2 bridge (Figs. 3a and 3b) can be replaced by a two-port network composed of two, galvanically separated and connected by $N_2:N_1$ ratio direct current sources $i_{d1(AV)}$ and $i_{d2(AV)}$. By treating all voltages and currents as averaged values for the period T and continuously changing over time, the considered DAB system can be presented in the form of an averaged model, consisting of a “DC transformer Tr ” and other elements corresponding to the real model, equipped with filters R_{E1} , L_{E1} , C_{E1} , and R_{E2} , L_{E2} , C_{E2} and surge protection circuits R_1 , C_1 , and R_2 , C_2 (Fig. 7).

The averaged model can be described by equations in which all voltages and currents are mean values over the period T , changing continuously as a function of time

$$L_{E1} \frac{di_{e1(AV)}}{dt} = e_{1(AV)} - v_{d1(AV)} - i_{e1(AV)} R_{E1}, \quad (16)$$

$$L_{E2} \frac{di_{e2(AV)}}{dt} = v_{d2(AV)} - e_{2(AV)} - i_{e2(AV)} R_{E2}, \quad (17)$$

Mathematical and simulation modeling of dual active bridge

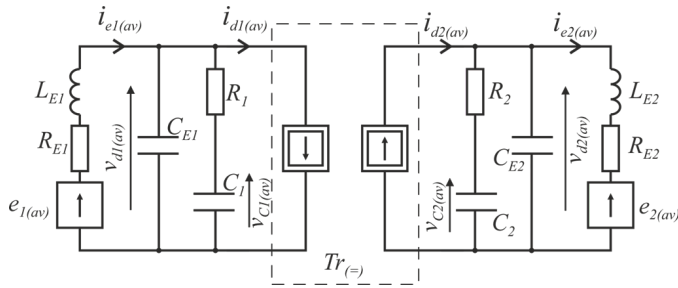


Fig. 7. Averaged large-signal model of DAB (large-signal model) with currents and voltages represented by mean values calculated over the period $T = T_s/2$

$$C_1 \frac{dv_{C1(AV)}}{dt} = \frac{1}{R_1} (v_{d1(AV)} - v_{C1(AV)}), \quad (18)$$

$$C_2 \frac{dv_{C2(AV)}}{dt} = \frac{1}{R_2} (v_{d2(AV)} - v_{C2(AV)}), \quad (19)$$

$$C_{E1} \frac{dv_{d1(AV)}}{dt} = i_{e1(AV)} - i_{d1(AV)} - \frac{1}{R_1} (v_{d1(AV)} - v_{C1(AV)}), \quad (20)$$

$$C_{E2} \frac{dv_{d2(AV)}}{dt} = i_{d2(AV)} - i_{e2(AV)} - \frac{1}{R_1} (v_{d2(AV)} - v_{C2(AV)}). \quad (21)$$

In the averaged model, switching elements are not included. As a result, calculations using average values are faster than calculations using actual instantaneous values of currents and voltages.

3. SMALL-SIGNAL DAB CONVERTER MODEL

In the analysis of dynamic properties, and especially in the design of the DAB converter control system, the so-called small-signal model [7] is helpful.

When creating a small-signal model, the mean value for the period $T = T_s/2$ in the transient state is treated as the sum of the quiescent value that occurs in the steady state immediately before the transient state (Fig. 6) and the variable component, called the small-signal component. It is assumed that the small-signal components are much smaller than the corresponding initial (quiescent) components of the considered quantities. Examples of transient currents and voltages in the dual active bridge are shown in Fig. 8.

The mean values, composed of the initial (quiescent) mean value and the mean value of the small-signal component, are expressed by the following formulas:

$$e_{1(AV)} = E_1 + \tilde{e}_1, \quad (22)$$

$$e_{2(AV)} = E_2 + \tilde{e}_2, \quad (23)$$

$$d_{(AV)} = D + \tilde{d}, \quad (24)$$

$$i_{e1(AV)} = I_{E1} + \tilde{i}_{e1}, \quad (25)$$

$$i_{e2(AV)} = I_{E2} + \tilde{i}_{e2}, \quad (26)$$

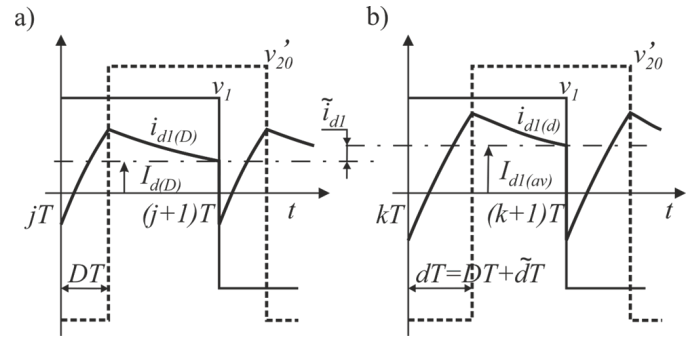


Fig. 8. Examples of AC voltage waveforms of transformer and DC circuit current in H_1 bridge circuit: a) initial steady state at control D in the range $jT < t < (j+1)T$; b) after changing the control by \tilde{d} in the range of $kT < t < (k+1)T$

$$i_{d1(AV)} = I_{d1} + \tilde{i}_{d1}, \quad (27)$$

$$i_{d2(AV)} = I_{d2} + \tilde{i}_{d2}, \quad (28)$$

$$v_{d1(AV)} = V_{d1} + \tilde{v}_{d1}, \quad (29)$$

$$v_{d2(AV)} = V_{d2} + \tilde{v}_{d2}, \quad (30)$$

$$v_{C1(AV)} = V_{C1} + \tilde{v}_{C1}, \quad (31)$$

$$v_{C2(AV)} = V_{C2} + \tilde{v}_{C2}, \quad (32)$$

where: $E_1, E_2, V_{d1}, V_{d2}, V_{C1}, V_{C2}, I_{E1}, I_{E2}, I_{d1}, I_{d2}, D$ – initial mean values (quiescent values) of the corresponding voltages, currents, and the control factor in the initial state, immediately before the occurrence of the transient state; $\tilde{e}_1, \tilde{e}_2, \tilde{v}_{d1}, \tilde{v}_{d2}, \tilde{v}_{C1}, \tilde{v}_{C2}, \tilde{i}_{e1}, \tilde{i}_{e2}, \tilde{i}_{d1}, \tilde{i}_{d2}, \tilde{d}$ – small-signal components (superimposed small ac variations) of voltages, currents, and the control factor.

The equations describing the small-signal model are obtained by substituting the formulas (22)–(32) for the formulas (16)–(21), taking into account only the components of the small AC variations. These equations take the following form:

$$L_{E1} \frac{d\tilde{i}_{e1}}{dt} = \tilde{e}_1 - \tilde{u}_{d1} - \tilde{i}_{e1} R_{E1}, \quad (33)$$

$$L_{E2} \frac{d\tilde{i}_{e2}}{dt} = \tilde{u}_{d2} - \tilde{e}_2 - \tilde{i}_{e2} R_{E2}, \quad (34)$$

$$C_1 \frac{d\tilde{v}_{C1}}{dt} = \frac{1}{R_1} (\tilde{v}_{d1} - \tilde{v}_{C1}), \quad (35)$$

$$C_2 \frac{d\tilde{v}_{C2}}{dt} = \frac{1}{R_2} (\tilde{v}_{d2} - \tilde{v}_{C2}), \quad (36)$$

$$C_{E1} \frac{d\tilde{v}_{d1}}{dt} = \tilde{i}_{e1} - \tilde{i}_{d1} - \frac{1}{R_1} (\tilde{v}_{d1} - \tilde{v}_{C1}), \quad (37)$$

$$C_{E2} \frac{d\tilde{v}_{d2}}{dt} = \tilde{i}_{d2} - \tilde{i}_{e2} - \frac{1}{R_1} (\tilde{v}_{d2} - \tilde{v}_{C2}). \quad (38)$$

When solving the equations describing the small-signal model, we obtain products of variable components of various quantities and components in the second and higher powers, which should be omitted as ridiculously small [16]. In order to linearize the model, an exponential expansion of the form $e^{a\tilde{d}}$ Taylor series

is used, from which for minor changes \tilde{d} we obtain [22]:

$$e^{\alpha\tilde{d}} \approx 1 + \alpha\tilde{d}, \quad (39)$$

where α is a constant.

Continuously changing small-signal mean values of currents (calculated for the period $T = T_s/2$) in the DC voltage circuits of both bridges \tilde{i}_{d1} and \tilde{i}_{d2} can be expressed by the formula:

$$\begin{bmatrix} \tilde{i}_{d1} \\ \tilde{i}_{d2} \end{bmatrix} = \begin{bmatrix} M_{11} & M_{12} & M_{13} \\ M_{21} & M_{22} & M_{23} \end{bmatrix} \begin{bmatrix} \tilde{d} \\ \tilde{v}_{d1} \\ \tilde{v}_{d2} \end{bmatrix}, \quad (40)$$

where:

$$M_{11} = \frac{2V_{d2}}{nR_z} \left(1 - \frac{2xy}{1+x} \right), \quad (41)$$

$$M_{12} = \frac{1}{R_{eq}} \left[1 + \frac{2\tau(x-1)}{T(1+x)} \right], \quad (42)$$

$$M_{13} = \frac{1}{nR_{eq}} \left[2D - 1 + \frac{2\tau(x-2xy+1)}{T(1+x)} \right], \quad (43)$$

$$M_{21} = \frac{2V_{d1}}{R_{eq}} \left(\frac{2y}{1+x} - 1 \right), \quad (44)$$

$$M_{22} = \frac{1}{R_{eq}} \left[1 - 2D + \frac{2\tau(x-2y+1)}{T(1+x)} \right], \quad (45)$$

$$M_{23} = \frac{1}{nR_{eq}} \left[\frac{2\tau(1-x)}{T(1+x)} - \frac{R_{eq} + R_m}{R_m} \right], \quad (46)$$

where: $x = e^{-T/\tau}$; $y = e^{-DT/\tau}$.

The small-signal model of the DAB converter can be represented using the same scheme as the large-signal model, except that the corresponding voltages and currents should be replaced by their variable low-signal components (Fig. 9). The two current sources in this model have values tied by the transformer ratio and are determined by the formulas (40)–(46).

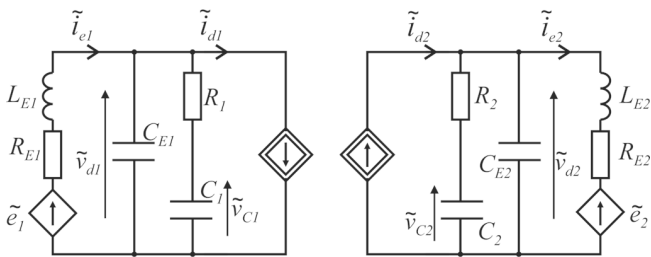


Fig. 9. Small-signal model of the DAB system with currents and voltages represented by the mean values of the variable components calculated for the period $T = T_s/2$

4. TRANSMITTANCE MODEL OF THE DAB SYSTEM TAKING INTO ACCOUNT PARASITIC PARAMETERS

The linearized small-signal model can be used to analyze the considered system in the field of complex pulsation s , including the determination of different transmittances. From the point

of view of the impact on the value of energy transmitted by the DAB system, transmittances linking the control signal d to currents i_{e1} and i_{e2} in the DC circuits of both bridges are the most interesting. That is because average values I_{E1} and I_{E2} multiplied by constant voltages E_1 and E_2 in these circuits are equal to the transmitted powers [3].

Assuming that the AC (low-signal) components of the voltages of the coupled DC circuits are zero $\tilde{e}_1(s) \approx 0$, $\tilde{e}_2(s) \approx 0$ based on equations (40)–(46), the following transmittances [16] are obtained:

- “control - to - input”

$$\begin{aligned} G_{i1/d}(s) &= \frac{\tilde{i}_{e1}(s)}{\tilde{d}(s)} \\ &= \frac{1}{R_{E1} + L_{E1}s} \cdot \frac{M_{13}M_{21}/G_2(s) + nM_{11}}{nG_1(s) + M_{21}M_{22}/G_2(s)}, \end{aligned} \quad (47)$$

- “control - to - output”

$$\begin{aligned} G_{i2/d}(s) &= \frac{\tilde{i}_{e2}(s)}{\tilde{d}(s)} \\ &= \frac{1}{R_{E2} + L_{E2}s} \cdot \frac{M_{21} - M_{11}M_{22}/G_1(s)}{nG_2(s) + M_{13}M_{22}/G_1(s)}, \end{aligned} \quad (48)$$

where:

$$G_1(s) = \frac{1}{R_1} + C_{E1}s + \frac{1}{F_1} + M_{12} - \frac{1/R_1}{1 + R_1C_1s}, \quad (49)$$

$$G_2(s) = \frac{1}{R_2} + C_{E2}s + \frac{1}{F_2} - \frac{M_{23}}{n} - \frac{1/R_2}{1 + R_2C_2s}. \quad (50)$$

Block diagrams of transmittance models corresponding to (40) and (47)–(50) are shown in Fig. 10.

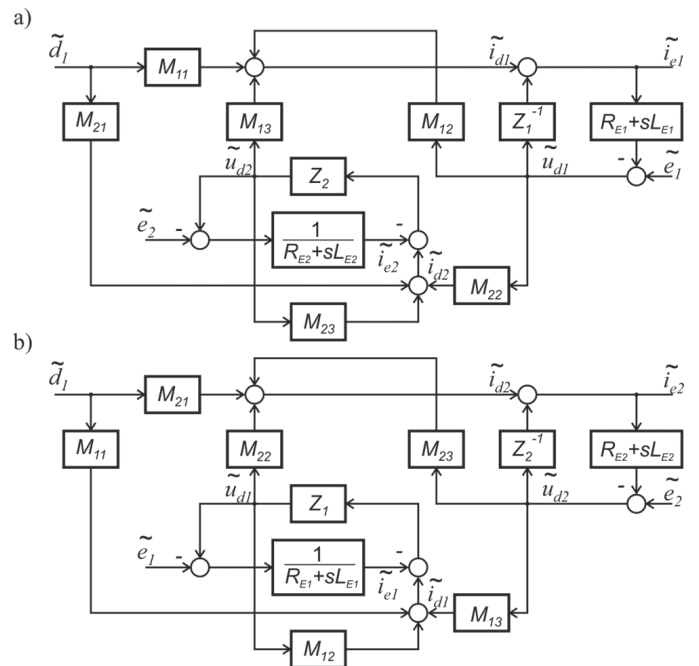


Fig. 10. Flowcharts of transmittance models taking into account parasitic parameters: a) “control - to - input”; b) “control - to - output”

5. AVERAGED DAB MODELS WITH IDEAL COMPONENTS

In order to assess the validity of considering parasitic resistances, a large-signal averaged mathematical model of the DAB system with ideal elements was also analyzed (Fig. 1). Omitting the surge protection circuits (R_1C_1 and R_2C_2) and all parasitic resistances and inductances, the diagram of the DAB system transferring electricity between the actual voltage sources e_1 and e_2 can be shown in Fig. 11.

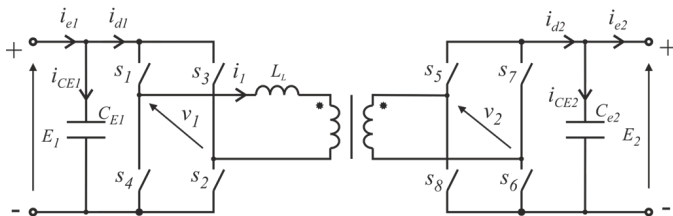


Fig. 11. DAB scheme with ideal components

Assuming that voltage sources e_1 and e_2 , besides the constant components E_1 and E_2 , can also have pulsed components, formula (1) can be written using time-varying quantities averaged over the period $T_s/2$ [16]:

$$p_{(AV)} = \frac{e_{1(AV)}e_{1(AV)}}{n2\pi f_s L_{eq}} d_{(AV)} (1 - d_{(AV)}) = ke_{1(AV)}e_{2(AV)}d_{(AV)} (1 - d_{(AV)}), \quad (51)$$

where $k = (n2\pi f_s L_{eq})^{-1}$.

Excluding power losses in the system, the powers on both sides of the DAB system are equal, i.e.

$$e_{1(AV)}i_{d1(AV)} = e_{2(AV)}i_{d2(AV)}. \quad (52)$$

Based on formulas (51) and (52), equations (2) and (3) take the form:

$$i_{d1(AV)} = kd_{(AV)} (1 - d_{(AV)}) e_{2(AV)}, \quad (53)$$

$$i_{d2(AV)} = kd_{(AV)} (1 - d_{(AV)}) e_{1(AV)}. \quad (54)$$

Considering the diagram in Fig. 11 and relationships (53) and (54), the large-signal ideal averaged model can be shown in Fig. 12.

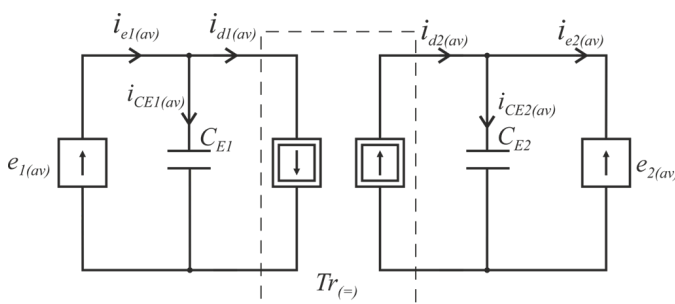


Fig. 12. Averaged DAB large-signal model with ideal components

In the case of the averaged large-signal model, the voltages and currents changing as a function of time, which are the sum of the initial values and the small mean values in the individual pulsed periods, are described by the formulas (22)–(28), which in the case take the following form:

$$e_{1(AV)} = E_1 + \tilde{e}_1, \quad e_{2(AV)} = E_2 + \tilde{e}_2,$$

$$d_{(AV)} = D + \tilde{d},$$

$$i_{e1(AV)} = I_{E1} + \tilde{i}_{e1}, \quad i_{e2(AV)} = I_{E2} + \tilde{i}_{e2},$$

$$i_{d1(AV)} = I_{d1} + \tilde{i}_{d1}, \quad i_{d2(AV)} = I_{d2} + \tilde{i}_{d2}.$$

The basic equations describing the large-signal averaged model of the DAB system with ideal elements can be written as:

$$C_{E1} \frac{de_{1(AV)}}{dt} = i_{e1(AV)} - i_{d1(AV)}, \quad (55)$$

$$C_{E2} \frac{de_{2(AV)}}{dt} = i_{d2(AV)} - i_{e2(AV)}. \quad (56)$$

Equations (55) and (56) correspond to equations (20) and (21).

Based on relationship (52)–(54) is obtained:

$$\begin{bmatrix} \tilde{i}_{d1} \\ \tilde{i}_{d2} \end{bmatrix} = k \begin{bmatrix} N_{11} & N_{12} & 0 \\ N_{21} & 0 & N_{23} \end{bmatrix} \begin{bmatrix} \tilde{d} \\ \tilde{e}_2 \\ \tilde{e}_1 \end{bmatrix}, \quad (57)$$

where [18]:

$$N_{11} = (1 - 2D)E_2, \quad (58)$$

$$N_{12} = N_{23} = (1 - D)D, \quad (59)$$

$$N_{21} = (1 - 2D)E_1. \quad (60)$$

Taking into consideration only the low-signal components equations (55) and (56) can be written as:

$$C_{E1} \frac{d\tilde{e}_1}{dt} = \tilde{i}_{CE1} = \tilde{i}_{e1} - \tilde{i}_{d1}, \quad (61)$$

$$C_{E2} \frac{d\tilde{e}_2}{dt} = \tilde{i}_{CE2} = \tilde{i}_{d2} - \tilde{i}_{e2} \quad (62)$$

or in the field of the complex variable s

$$\tilde{e}_1(s) = \frac{1}{sC_{E1}} (\tilde{i}_{e1}(s) - \tilde{i}_{d1}(s)), \quad (63)$$

$$\tilde{e}_2(s) = \frac{1}{sC_{E2}} (\tilde{i}_{d2}(s) - \tilde{i}_{e2}(s)). \quad (64)$$

From equations (57)–(64), the following transmittances are obtained:

$$G_{e1}^{\tilde{d}}(s) = \frac{\tilde{e}_1}{\tilde{d}} = \frac{sC_{E2}}{s^2C_{E1}C_{E2} + k^2N_{12}N_{23}} \cdot \left(-kN_{11} - + \frac{1}{sC_{E2}} k^2N_{12}N_{21} \right), \quad (65)$$

R. Barlik, P. Grzejszczak, and M. Koszel

$$G_{\frac{e_2}{d}}(s) = \frac{\tilde{e}_2}{\tilde{d}} = \frac{sC_{E1}}{s^2C_{E1}C_{E2} + k^2N_{12}N_{23}} \cdot \left(kN_{21} - + \frac{1}{sC_{E1}}k^2N_{11}N_{23} \right), \quad (66)$$

$$G_{ie1/d}(s) = \frac{\tilde{i}_{e2}}{\tilde{d}} = k(1 - 2D)E2, \quad (67)$$

$$G_{ie2/d}(s) = \frac{\tilde{i}_{e1}}{\tilde{d}} = k(1 - 2D)E1. \quad (68)$$

The low-signal models of the DAB system in the time and complex s variable fields are shown in Fig. 13.

6. SIMULATION MODEL

The simulation model was developed in the PLECS environment in two versions: with parasitic components and ideal (Figs. 14a and 14b) according to Section 2 and Section 5, respectively. The model was developed to check the accordance of the transfer function model with the circuit model by investigating the open and close loop step responses of both models.

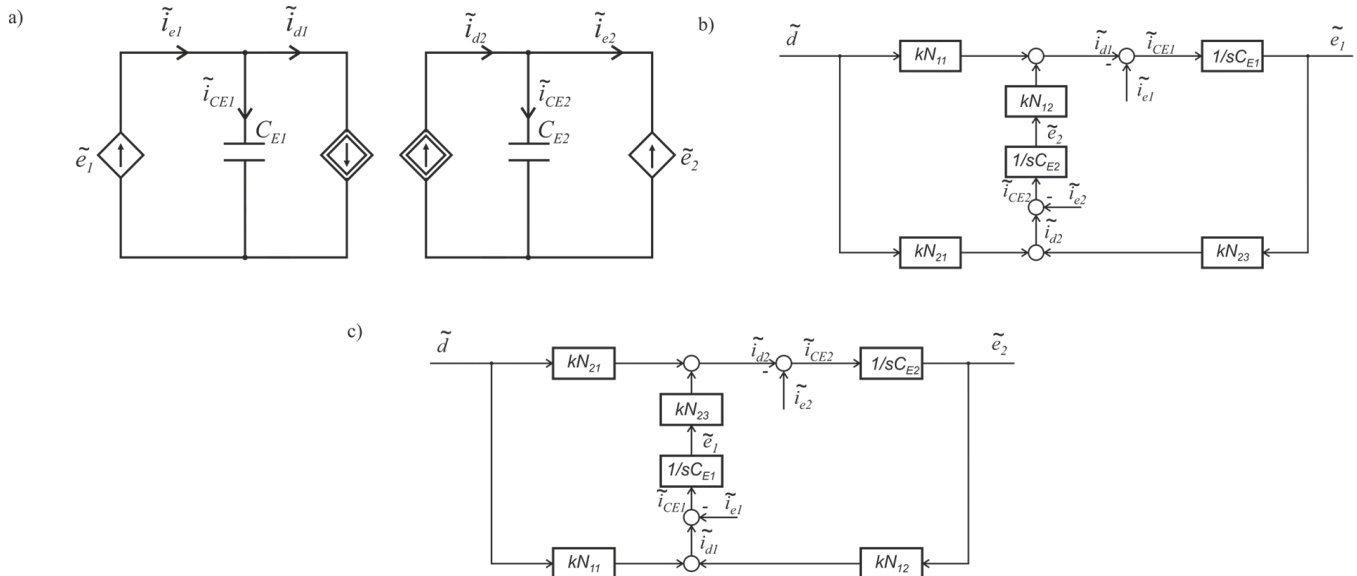


Fig. 13. A small-signal model of the DAB system with ideal elements: a) a diagram with quantities in the time field; b) transmittance model “control - to - input”; c) transmittance model “control - to - output”

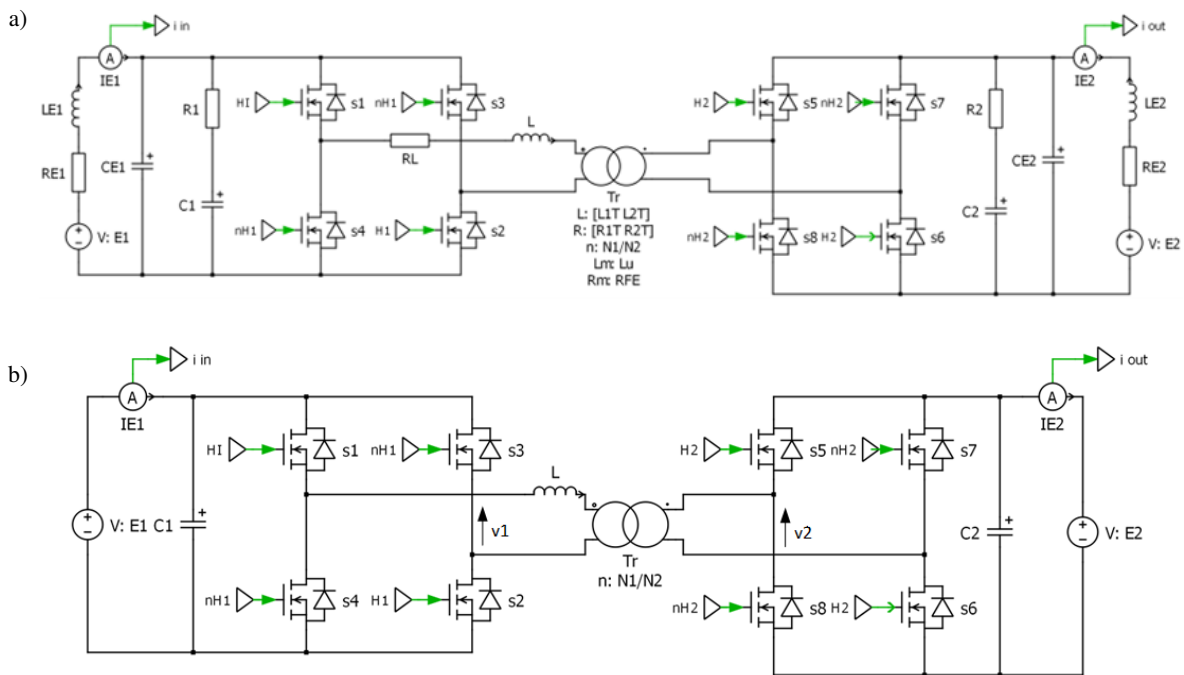


Fig. 14. PLECS simulation schematic: a) model with parasitic parameters; b) ideal components

7. EXPERIMENTAL SETUP

To verify accordance with the transmittance models described by formulas (47) and (48) introduced in Section 4 experimental model was also developed. The main components of the model are SIC MOSFET transistors (s_1 – s_8), the planar transformer (Tr), and DC circuit capacity consisting of parallel connection of low ESR film (C_{E1} , C_{E2}) and electrolytic (C_1 , R_1 , C_2 , R_2) capacitors. DC lowpass LC input and output current filters (L_{E1} , R_{E1} , L_{E2} , R_{E2}) were also included. The control algorithm was designed on the CYC1000 board created around Intel Cyclone 10 LP FPGA. The switching frequency was 100 kHz with 125 ns dead time, whereas the controller sampling frequency was five times higher than the transistor switching frequency. In Table 1, experimental model components are listed.

Table 1
Selected components

Component	Schematic model symbol	Parameters	
DTP-33	L_{E1}^* , L_{E2}^*	L_E 50Hz	110 uH
	R_{E1}^* , R_{E2}^*	R_E 50Hz	10 mΩ
MKP1848620094P4	C_{E1}	C	20 uF
		ESR	5 mΩ
MKP1848620704P4	C_{E2}	C	20 uF
		ESR	6 mΩ
HC2G107M22030HA18	C_1 , C_2	C	100 uF
	R_1 , R_2	R	1.6 Ω
C3M00120100K	s_1 – s_4	V_{DS}	1000 V
		I_D	22 A
		R_{ON}	120 mΩ
UF3C120150K4S	s_5 – s_8	V_{DS}	1200 V
		I_D	18.4 A
		R_{ON}	150mΩ
T1000AC-18-20	Tr	$N_2:N_1$	18:20
		I_{TRMS}	11.2 A
		L_{1T} 100kHz	4 uH
		R_{1T} 100kHz	37 mΩ
Own project	L	$L_{L100kHz}$	50 uH
		$R_{L100kHz}$	47 mΩ

where: L_{E50Hz} – inductance at 50 Hz, 1A; R_{E50Hz} – resistance at 50 Hz; ESR – equivalent series resistance; V_{DS} – nominal drain-source voltage; I_D – continuous drain current (case temperature, $T_c = 25^\circ\text{C}$); R_{ON} – drain-source resistance (case temperature, $T_c = 25^\circ\text{C}$); N_1 , N_2 – the number of turns of the transformer primary and secondary winding, respectively; I_{TRMS} – maximum RMS value of transformer primary current; L_{1T} 100kHz, R_{1T} 100kHz – transformer primary side leakage inductance and winding resistance at 100 kHz, respectively; L_μ – transformer magnetizing inductance; $L_{L100kHz}$, $R_{L100kHz}$ – inductor leakage inductance and resistance at 100 kHz, respectively.

* In the simulation and transfer function model, besides DC filter parameters (L_{E50Hz} , R_{E50Hz}), the resistance of wires connecting DAB and DC voltage source, the resistance of contactors, as well as filtering inductance of DC voltage power supply were also included. Total values of L_{E1} , L_{E2} were estimated as 200 uH and R_{E1} , R_{E2} as 60 mΩ.

The source of parameter values is the manufacturer’s datasheets and precise measurements conducted with the GW INSTEK LCR-8105G meter.

The experimental model and laboratory bench are illustrated in Fig. 15. The equipment used during tests consisted of an MDO3034 Tektronix oscilloscope with voltage probes THDP0200 and current probe TCP0030A, DP 832 Rigol DC power supply and two bidirectional DC power supplies IT6018B.

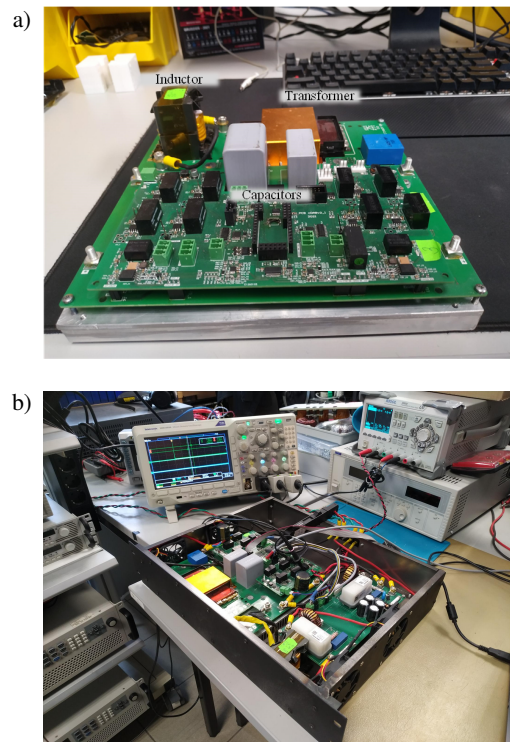


Fig. 15. Experimental research: a) model of the dual active bridge; b) research testbench

8. RESULTS

The aim of the simulation and experimental tests can be listed as:

- Checking accordance of open and close loop step response of transfer function model with the PLECS simulation model (Figs. 17 and 18).
- Checking accordance of open and close loop step response of transfer function model with the experimental model (Fig. 19).
- Design of PI controller based on transfer function model and its testing with different DC circuits voltage ratio, and different reference value (Figs. 20 and 21).

Because of the strict analogy between control-to-input and control-to-output transfer functions, only control-to-output one was verified in detail in simulation and experimental research.

Two operating points with different input-to-output voltage ratios were chosen for analysis. In the first one $E2' \approx E1$ (DC circuits voltage ratio $E2'/E1 \approx 1$), which results in trapezoidal i_L (Fig. 16a). In the second one $E2' \approx 1/3 E1$ (Fig. 16b), which results in nearly triangular i_L .

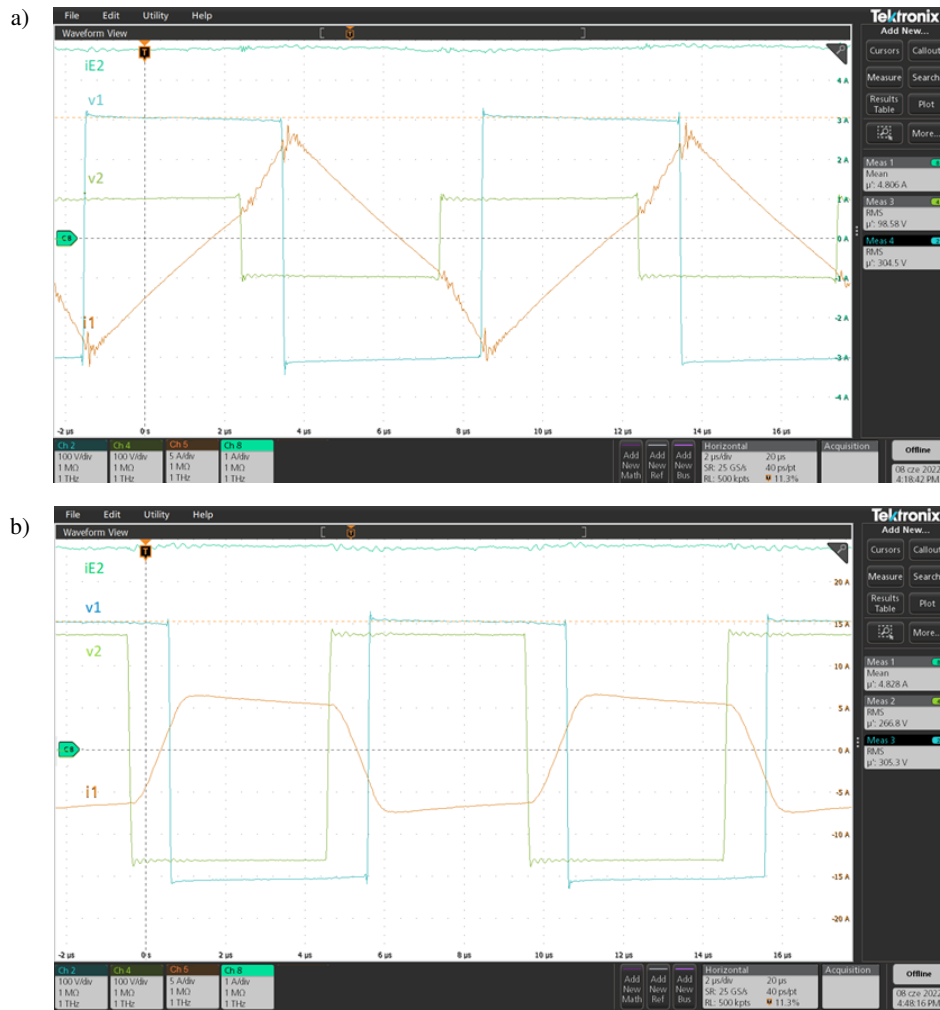


Fig. 16. Steady-state oscillogram of DAB experimental model – AC side voltages v_1 , v_2 (100 V/div), AC primary current (5 A/div) i_1 and output current of the converter i_{E2} (1 A/div): a) $E_1 = 300$ V, $E_2 = 100$ V, $i_{E2} = 5$ A; b) $E_1 = 300$ V, $E_2 = 270$ V, $i_{E2} = 5$ A

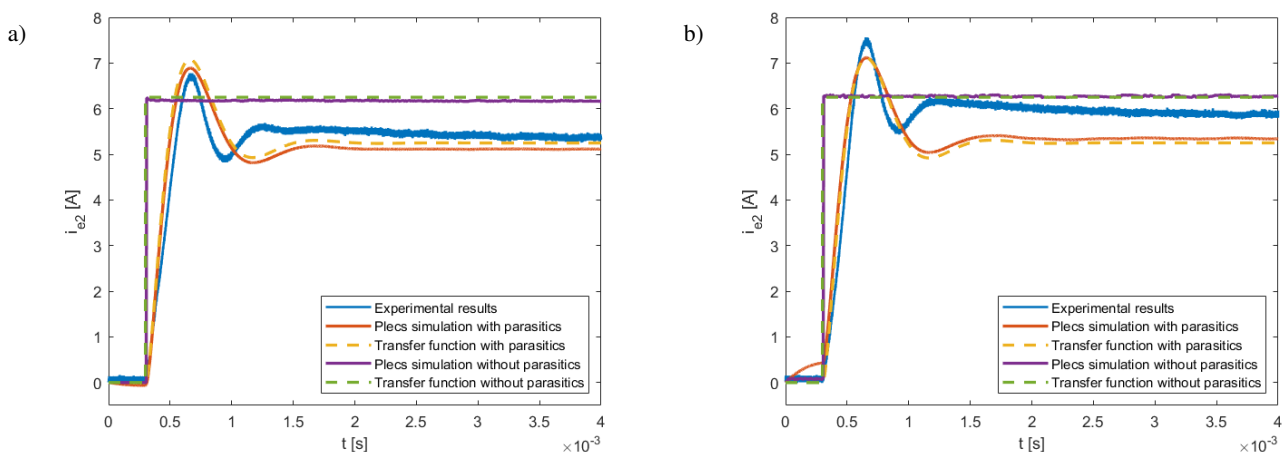


Fig. 17. Open loop step response output current transient: a) $d = T_s/8$, $E_1 = 300$ V, $E_2 = 270$ V; b) $d = T_s/8$, $E_1 = 300$ V, $E_2 = 100$ V

Secondly, close-loop step responses were examined. At first, the accordance with the closed loop of step response was checked (Fig. 19). Then the control-to-output transfer function

was used to optimize PI controller gains, which at the beginning were experimentally set with preliminary values according to the assumed shape of the closed-loop step response.

Mathematical and simulation modeling of dual active bridge

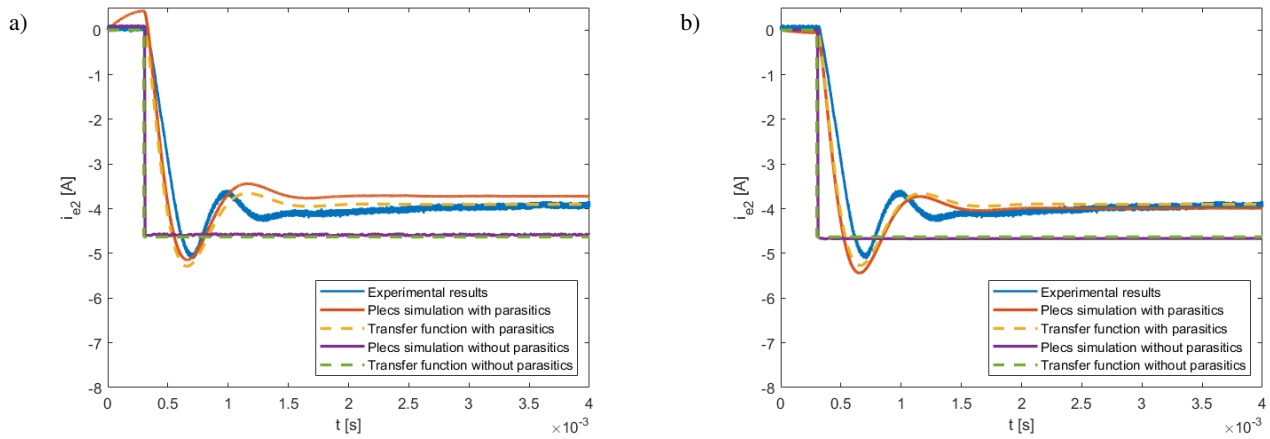


Fig. 18. Open loop step response (output current): a) $d = -T_s/12$, $E_1 = 300$ V, $E_2 = 100$ V; b) $d = -T_s/12$, $E_1 = 300$ V, $E_2 = 270$ V

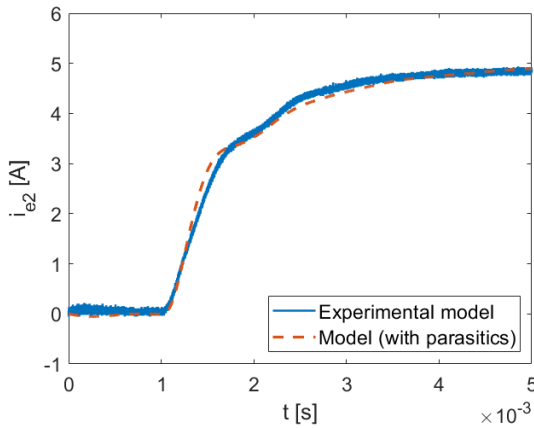


Fig. 19. Closed-loop step response output current with preliminary ($E_1 = 300$ V, $E_2 = 270$ V)

Transients shown in Figs. 17 and 18 present differences in step response received in tests with different models. Application of ideal transfer function and circuit models results in rectangular step response, where rise time and overshoot are neglected. The simplicity of such a model result in strict accordance with the PLECS simulation and transfer function model. The gain of ideal models is higher than in models with parasitic elements because all parasitic resistances responsible for power loss modeling are omitted. Including parasitic elements in simulation and small-signal analysis results in the possibility of modeling current dynamics precisely. Steady-state value is also modeled more accurately and close to that measured in experimental research. Some errors exist due to mitigating initial conditions and some of the parasitic components and non-ideal characteristics of DC power supply the transfer function model.

Another principal observation is the accordance with the PLECS simulation results with the small-signal transfer function model, which proves the possibility of replacing circuit simulation models with such based on the transfer function.

In Table 2 errors of models were presented.

Errors were calculated by formula (69), whereas the *measure* is a value of rise-time/overshoot/steady-state value/settling time

Table 2

Comparison of open loop step responses with reference to experimental model (case from Fig. 18a)

Model	Rise-time*	Overshoot	Steady-state value	Settling time**
PLECS simulation with parasitics (error)	34%	2%	5%	13%
Transfer function with parasitics (error)	27%	5%	0%	13%
PLECS simulation without parasitics (error)	–	–	17%	–
Transfer function without parasitics (error)	–	–	19%	–

* rise time – the time the response takes to rise from 10% to 90% of the way from the initial value to the steady-state value.

** settling-time – the time after that the response does differ from the steady-state value for more than 5%.

in step response of a model and the *reference* is a respective value in step response of the experimental model

$$\text{error} = \left| 1 - \frac{\text{measure}}{\text{reference}} \cdot 100\% \right|. \quad (69)$$

The table refers to traces presented in Fig. 18a.

In ideal models, only steady-value error was calculated because of negligible values of rise-time, overshoot, and settling-time in such models.

Closed-loop responses of the small-signal model and experimental results were also compared. Figure 19 presents the accordance of both transients in terms of rising time and steady-state value.

The coverage of experimental and simulation characteristics means that applying a detailed transfer function model facilitates choosing PI settings according to given parameters in the time or frequency domain.

The transmittance model can be used to design the controller of a converter [23]. In this case, a user-friendly Simulink Open PID Tuner was used. The tool facilitates tuning PI controller in

R. Barlik, P. Grzejszczak, and M. Koszel

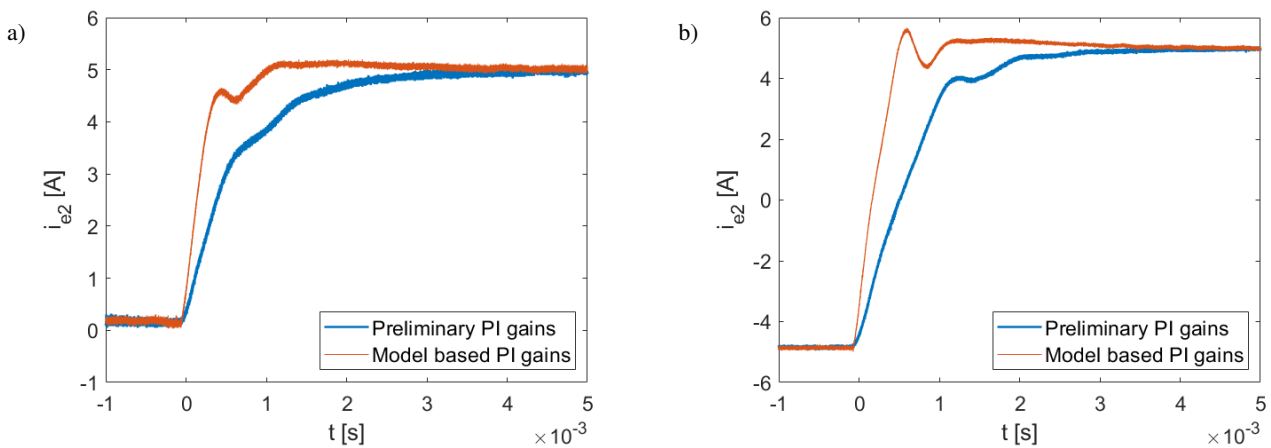


Fig. 20. Closed-loop step response output current i_{E2} ($E_1 = 300$ V, $E_2 = 270$ V): a) 0 to 5 A; b) -5 A to 5 A

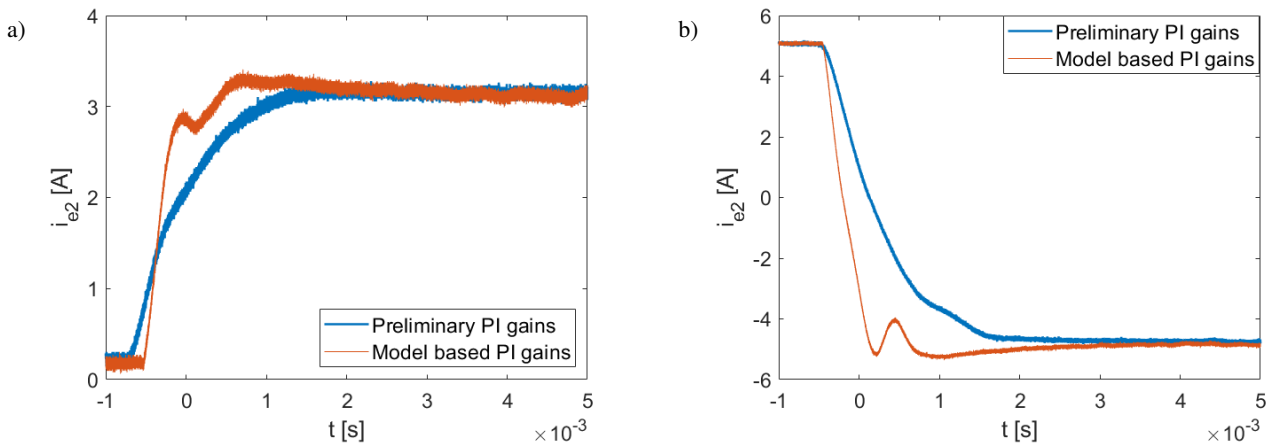


Fig. 21. Closed-loop step response output current i_{E2} ($E_1 = 300$ V, $E_2 = 100$ V): a) 0 to 3 A; b) 5 A to -5 A

Table 3

Pi controller settings

PI settings	Model-based tuning
P	2.53
I	33301
T_s	2 us

frequency and time domain. In this research time domain analysis during tuning, the requirement of a maximum 10% overshoot and minimum rising time was taken. The model-based chosen PI controller gains are presented in Table 3. The discrete equation of the PI controller is described by formula (70)

$$P + I \cdot T_s \cdot \frac{1}{z-1}. \quad (70)$$

Closed-loop step responses of the system with preliminary chosen PI gains (blue color) were compared with step responses of the system with model-based chosen PI gains (red color) in Figs. 20 and 21.

Step responses were compared for different values of reference current and DC voltages. The research was aimed at experimental verification of derived transfer functions and checking their usefulness in tuning PI controllers for dual active bridge converters.

9. CONCLUSIONS

In the paper, the dual active bridge model given in [16] was supplemented with threshold voltages of diodes and transistors as well as a leakage inductor inductance and AC resistance. Furthermore, the transfer function model open loop step response was compared with the Plescs simulation model and the experimental one in different conditions. The impact of variation of DC circuits voltage and the phase-shift coefficient on the accordance of the transfer function model and the experimental model was also discussed. Finally, the transfer function model was used to tune the PI controller according to set priorities.

The research included the models with two levels of accuracy: losses ideal one and the other including plenty of parasitic components.

The model of the converter allows for a more precise representation of dynamic states because of including additional parasitic components in the analysis. Transfer function takes into account numerous parasitic components models, input, and output of current transients of a dual active bridge converter accurately. The discrepancies result from the limitation of the model, inaccuracy in determining the values of the parameters, and not taking all parasitic parameters into account. Nevertheless, the accuracy of the level of PLECS circuit simulation is achieved, which predisposes this model to be used in modeling complex systems, resulting in simplification of the model while maintaining the properties of the entire system. The introduced model can contribute to speeding up simulation research. Appropriate mapping of dynamic states allows the model to be used to design controllers.

It should be noted that besides accurate representation of the real system, the transfer function model is limited to a given operating point. Maintaining a strict link to actual working conditions requires recalculating when parameters change.

The use of the small-signal model allows for a quick and straightforward selection of adjustments to the parameters of the regulators while maintaining a high level of representation of the physical model.

APPENDIX

After entering the designation $D_0 = 1 - D$, depending (53) and (54) are obtained

$$\begin{aligned}
 I_{d1} + \tilde{i}_{d1} &= k(D + \tilde{d})(1 - D - \tilde{d})(E_2 + \tilde{e}_2) \\
 &= k(D + \tilde{d})(D_0 - \tilde{d})(E_2 + \tilde{e}_2) = \\
 &= \left(kDD_0 - kD\tilde{d} + k\tilde{d}D_0 - k(\tilde{d})^2\right)(E_2 + \tilde{e}_2) \\
 &= kDD_0E_2 + kDD_0\tilde{e}_2 - kD\tilde{d}E_2 - kD\tilde{d}\tilde{e}_2 \\
 &+ k\tilde{d}D_0E_2 + k\tilde{d}D_0\tilde{e}_2 - \left(k(\tilde{d})^2E_2 - k(\tilde{d})^2\tilde{e}_2\right). \quad (71)
 \end{aligned}$$

By eliminating components in which there are the products of small values, i.e. $\tilde{d}\tilde{e}_2$; \tilde{d}^2 and $\tilde{d}^2\tilde{e}_2$, we obtain

$$\begin{aligned}
 I_{d1} + \tilde{i}_{d1} &= kDD_0E_2 + kDD_0\tilde{e}_2 - kDE_2\tilde{d} + kD_0E_2\tilde{d} \\
 &= \tilde{d}(kD_0E_2 - kDE_2) + \tilde{e}_2kDD_0 \\
 &= k(\tilde{d}(1 - 2D)E_2 + \tilde{e}_2D(1 - D)) \\
 &= k(\tilde{d}N_{11} + \tilde{e}_2N_{12}) \quad (72)
 \end{aligned}$$

and

$$\begin{aligned}
 I_{d2} + \tilde{i}_{d2} &= k(D + \tilde{d})(1 - D - \tilde{d})(E_1 + \tilde{e}_1) \\
 &= k(D + \tilde{d})(D_0 - \tilde{d})(E_1 + \tilde{e}_1) \\
 &= \left(kDD_0 - kD\tilde{d} + k\tilde{d}D_0 - k(\tilde{d})^2\right)(E_1 + \tilde{e}_1) \\
 &= kDD_0E_1 + kDD_0\tilde{e}_1 - kD\tilde{d}E_1 - kD\tilde{d}\tilde{e}_1 + k\tilde{d}D_0E_1 \\
 &+ k\tilde{d}D_0\tilde{e}_1 - \left(k(\tilde{d})^2E_1 + k(\tilde{d})^2\tilde{e}_1\right). \quad (73)
 \end{aligned}$$

By eliminating components in which are the products of small values, i.e. $\tilde{d}\tilde{e}_1$; \tilde{d}^2 and $\tilde{d}^2\tilde{e}_1$, we obtain

$$\begin{aligned}
 \tilde{i}_{d2} &= \tilde{d}(kD_0E_1 - kDE_1) + \tilde{e}_1kDD_0 \\
 &= k(\tilde{d}(1 - 2D)E_1 + \tilde{e}_1D(1 - D)) \\
 &= k(\tilde{d}N_{21} + \tilde{e}_2N_{23}). \quad (74)
 \end{aligned}$$

ACKNOWLEDGEMENTS

The research was supported by The National Centre for Research and Development (NCBR) grant number MAZOWSZE/0111/19 “SIMES – Smart Integrated Modular Energy System for DC microgrids with renewable energy sources and energy storage”.

REFERENCES

- [1] D.-K. Jeong, H.-S. Kim, J.-W. Baek, J.-Y. Kim, and H.-J. Kim, “Dual active bridge converter for energy storage system in DC microgrid,” 2016 *IEEE Transportation Electrification Conference and Expo, Asia-Pacific (ITEC Asia-Pacific)*, 2016, pp. 152–156, doi: [10.1109/ITEC-AP.2016.7512939](https://doi.org/10.1109/ITEC-AP.2016.7512939).
- [2] M.-S. Kim, D.-H. Kim, D.-K. Jeong, J.-M. Kim, and H.-J. Kim, “Soft start-up control strategy for dual active bridge converter with a supercapacitor,” *Energies*, vol. 13, no. 16, p. 4083, Aug. 2020, doi: [10.3390/en13164083](https://doi.org/10.3390/en13164083).
- [3] R. Barlik, M. Nowak, and P. Grzejszczak, “Power transfer analysis in a single phase dual active bridge,” *Bull. Pol. Acad. Sci. Tech. Sci.*, vol. 61, no. 4, pp. 809–828, 2013. doi: [10.2478/bpasts-2013-0088](https://doi.org/10.2478/bpasts-2013-0088).
- [4] Y. Xiao, Z. Zhang, K.T. Manez, and M.A.E. Andersen, “A universal power flow model for dual active bridge-based converters with phase shift modulation,” *IEEE Trans. Power Electron.*, vol. 36, no. 6, pp. 6480–6500, June 2021, doi: [10.1109/TPEL.2020.3039195](https://doi.org/10.1109/TPEL.2020.3039195).
- [5] K. Takagi and H. Fujita, “Dynamic control and performance of a dual-active-bridge DC-DC converter,” *IEEE Trans. Power Electron.*, vol. 33, no. 9, pp. 7858–7866, Sept. 2018, doi: [10.1109/TPEL.2017.277326](https://doi.org/10.1109/TPEL.2017.277326).
- [6] S. Shao *et al.*, “Modeling and advanced control of dual-active-bridge DC-DC converters: A review,” *IEEE Trans. Power Electron.*, vol. 37, no. 2, pp. 1524–1547, Feb. 2022, doi: [10.1109/TPEL.2021.3108157](https://doi.org/10.1109/TPEL.2021.3108157).
- [7] Y. Yan, H. Gui, and H. Bai, “Complete ZVS analysis in dual active bridge,” in *IEEE Trans. Power Electron.*, vol. 36, no. 2, pp. 1247–1252, Feb. 2021, doi: [10.1109/TPEL.2020.3011470](https://doi.org/10.1109/TPEL.2020.3011470).
- [8] H. Qin and J. W. Kimball, “Generalized average modeling of dual active bridge DC-DC converter,” *IEEE Trans. Power Electron.*, vol. 27, no. 4, pp. 2078–2084, Apr. 2012, doi: [10.1109/TPEL.2011.2165734](https://doi.org/10.1109/TPEL.2011.2165734).
- [9] R.W. Erickson and D. Maksimovic, *Fundamentals of Power Electronics*. 2ed., Springer, 2001.
- [10] W. Janke, “Equivalent circuits for averaged description of DC-DC switch mode converters based on separation of variables approach,” *Bull. Pol. Acad. Sci. Tech. Sci.*, vol. 61, no. 3, pp. 711–723, 2013. doi: [10.2478/bpasts-2013-0076](https://doi.org/10.2478/bpasts-2013-0076).
- [11] O.M. Hebala, A.A. Aboushady, K.H. Ahmed, S. Burgess, and R. Prabhu, “Generalized small-signal modelling of dual active bridge DC/DC converter,” 2018 *7th International Conference on Renewable Energy Research and Applications (ICRERA)*, 2018, pp. 914–919, doi: [10.1109/ICRERA.2018.8567014](https://doi.org/10.1109/ICRERA.2018.8567014).

- [12] F.L.F. Marcelino, H.H. Sathler, T.R. de Oliveira, and P.F. Donoso-Garcia, "Modeling and control of a dual active bridge for energy storage in DC microgrid applications," 2017 *IEEE 8th International Symposium on Power Electronics for Distributed Generation Systems (PEDG)*, 2017, pp. 1–8, doi: [10.1109/PEDG.2017.7972461](https://doi.org/10.1109/PEDG.2017.7972461).
- [13] I. Batarseh and K. Siri, "Generalized approach to the small-signal modeling of DC-to-DC resonant converters," *IEEE Trans. Aerosp. Electron. Syst.*, vol. 29, no. 3, pp. 894–909, July 1993, doi: [10.1109/7.220938](https://doi.org/10.1109/7.220938).
- [14] P. Wang, X. Chen, C. Tong, P. Jia, and C. Wen, "Large- and small-signal average-value modeling of dual-active-bridge DC-DC converter with triple-phase-shift control," *IEEE Trans. Power Electron.*, vol. 36, no. 8, pp. 92379250, Aug. 2021, doi: [10.1109/TPEL.2021.3052459](https://doi.org/10.1109/TPEL.2021.3052459).
- [15] F. Krismer and J. W. Kolar, "Accurate small-signal model for the digital control of an automotive bidirectional dual active bridge," *IEEE Trans. Power Electron.*, vol. 24, no. 12, pp. 2756–2768, Dec. 2009, doi: [10.1109/TPEL.2009.2027904](https://doi.org/10.1109/TPEL.2009.2027904).
- [16] K. Zhang, Z. Shan, and J. Jatskevich, "Large- and small-signal average-value modeling of dual-active-bridge DC-DC converter considering power losses," *IEEE Trans. Power Electron.*, vol. 32, no. 3, pp. 1964–1974, March 2017, doi: [10.1109/TPEL.2016.2555929](https://doi.org/10.1109/TPEL.2016.2555929).
- [17] H. Beiranvand, E. Rorok, and M. Liserre, "Theoretical evaluation of semiconductor loss components behavior in ISOP-DAB converters," 2019 *IEEE 13th International Conference on Compatibility, Power Electronics and Power Engineering (CPE-POWERING)*, 2019, pp. 1–7, doi: [10.1109/CPE.2019.8862369](https://doi.org/10.1109/CPE.2019.8862369).
- [18] T.N. Ramasamy, "Power Device Loss Analysis of a High-Voltage High-Power Dual Active Bridge DC-DC Converter," *Electric Power Conversion*, Ed. M. Găiceanu, IntechOpen, 2018, doi: [10.5772/intechopen.80696](https://doi.org/10.5772/intechopen.80696). [Online] Available: <https://www.intechopen.com/chapters/63379>.
- [19] J. Liu, J. Yang, J. Zhang, Z. Nan, and Q. Zheng, "Voltage balance control based on dual active bridge DC/DC converters in a power electronic traction transformer," *IEEE Trans. Power Electron.*, vol. 33, no. 2, pp. 1696–1714, Feb. 2018, doi: [10.1109/TPEL.2017.2679489](https://doi.org/10.1109/TPEL.2017.2679489).
- [20] R. Barlik, P. Grzejszczak, and M. Zdanowski, "Determination of the basic parameters of the high-frequency planar transformer," *Prz. Elektrotechniczny. – Electr. Rev.*, vol. R. 92, no. 6, pp. 71–78, 2016. doi: [10.15199/48.2016.06.13](https://doi.org/10.15199/48.2016.06.13).
- [21] J.G. Kassakian, M.F. Schlecht, and G.C. Verghese, *Principles of Power Electronics*. Addison – Wesley Publishing Company, Massachusetts Institute of Technology, 1999.
- [22] M.M. Garg, Y.V. Hote, M.K. Pathak, and L. Behera, "An approach for buck converter PI controller design using stability boundary locus," 2018 *IEEE/PES Transmission and Distribution Conference and Exposition (T&D)*, 2018, pp. 1–5, doi: [10.1109/TDC.2018.8440291](https://doi.org/10.1109/TDC.2018.8440291).
- [23] D. Xue, Y.Q. Chen, and D.P. Atherton, *Linear Feedback Control*, 2007, pp. 183–235.